Toward a dual-species atom interferometer with cadmium and strontium

Towards a dual-species atom interferometer with cadmium and strontium

J. N. Tinsley,[1,2] S. Bandarupally,[1] M. Chiarotti,[1,3] S. Manzoor,[1,a)] M. Sacco,[1] and N. Poli[1,3]
[1)]*Dipartimento di Fisica e Astronomia and LENS, Università degli Studi di Firenze, Via G. Sansone 1, 50019 – Sesto Fiorentino, Italy*
[2)]*Department of Physics, University of Liverpool, Oliver Lodge Laboratory, Oxford Street, Liverpool, L69 7ZE, UK*
[3)]*CNR-INO, Via Nello Carrara 1, 50019 – Sesto Fiorentino, Italy*

(*Electronic mail: nicola.poli@unifi.it)

(Dated: 29 February 2024)

We report on the progress towards a dual-species cadmium and strontium atom interferometer for fundamental physics tests. We have developed and characterised a complete baseline laser system for cadmium, which provides the high power and narrow linewidth necessary for laser cooling and trapping and for performing atom interferometry, with upgraded systems for strontium also implemented. An overview of a design for cooling cadmium is presented and we outline the basic design of a Cd-Sr atomic fountain, discussing atom launching techniques and the possible role of blackbody radiation. The excellent properties of cadmium and strontium, both individually and as a test pair, are discussed along with the enabled fundamental physics programme of tests of the weak equivalence principle and the measurement of relativistic time dilation effects in quantum superpositions of clocks.

I. INTRODUCTION

Contemporary atomic clocks and atom interferometers provide measurements of frequency and gravity with unprecedented precision[1,2], arising from the possibility to control both internal and external degrees of freedom combined with matter wave's sensitivity to electromagnetic and gravitational fields[3,4]. Atom interferometers based on the intercombination transitions of alkaline-earth and alkaline-earth-like atoms operate at the intersection of these two devices and represent an emerging technology[5–9] with a broad range of applications for fundamental physics tests. In particular, much attention has recently been focused on atom interferometers based on the $^1S_0$-$^3P_0$ clock transition of strontium[7,8], for which large baseline (≥ 10 m) devices are currently under construction in the UK, the USA and China[10–12]. These experiments aim to search for ultralight dark matter and mid-band gravitational waves, amongst other goals, and may serve as landmarks for future space-based missions[13,14].

Strontium, however, is not the only species suitable for such experiments, with ytterbium also receiving considerable attention. A further interesting candidate is atomic cadmium which possesses a similar electronic energy level structure to strontium, but with ground-state transitions approximately double in frequency, placing them within the ultraviolet region (see Fig. 1). This provides numerous potential advantages, including higher intrinsic momentum transfer and reduced sensitivity to blackbody radiation. Shorter wavelengths also have an increased Rayleigh length, leading to better wave front and intensity homogeneity throughout the interferometry region and reducing the effect of the Gouy phase[15].

Here we report on the progress towards a new dual-species atom interferometer, based on cadmium and strontium atoms, detailing the key design considerations and physics goals. In brief, however, a complete baseline laser system for cadmium has been developed and characterised, as well as upgraded laser systems for strontium, as presented in Section III. More details on cadmium and strontium are first presented in Section II, as well as the fundamental physics programme of the dual-species interferometer. The basic cold atom apparatus and some key systematic considerations are presented in Section IV, before conclusions and future plans are presented in Section V.

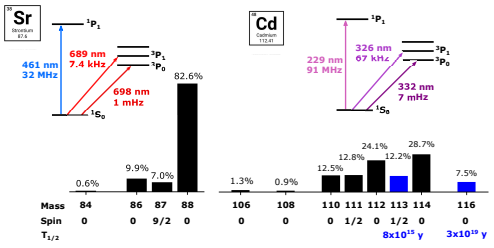

FIG. 1. The main transitions of interest for strontium and cadmium and information on the naturally occurring isotopes. More details can be found in Table I and Section II A.

II. A CD-SR ATOM INTERFEROMETER

A. Relevant properties of cadmium and strontium

Strontium and cadmium are divalent atoms meaning they provide access to both broad dipole-allowed transitions and narrow forbidden intercombination transitions, as summarised in Fig. 1 and Table I. This combination provides the capability for both efficient cooling and trapping down to the μK level in magneto-optical traps (MOTs) and the possibility to perform high-precision measurements in the optical regime. For the

[a)]Present address: Department of Experimental Physics, Comenius University, Mlynská dolina, Bratislava 842 48, Slovakia

TABLE I. Properties of the transitions of Cd and Sr atoms shown in Fig. 1. Reported values are for the wavelength (λ), natural linewidth (Γ), saturation intensity (I_s) and Doppler temperature (T_D).

	Transition	λ (nm)	$\Gamma/2\pi$	I_s (mW/cm^2)	T_D
	$^1S_0$-$^1P_1$	228.8	91 MHz	992	2.2 mK
Cd	$^1S_0$-$^3P_1$	326.1	67 kHz	0.252	1.6 μK
	$^1S_0$-$^3P_0$	332.1	7 mHz (^{111}Cd, ^{113}Cd)	$\sim 10^{-9}$	–
	Transition	λ (nm)	$\Gamma/2\pi$	I_s (mW/cm^2)	T_D
	$^1S_0$-$^1P_1$	460.9	32 MHz	42.5	0.7 mK
Sr	$^1S_0$-$^3P_1$	689.4	7.4 kHz	3×10^{-3}	180 nK
	$^1S_0$-$^3P_0$	698.4	1 mHz (^{87}Sr)	$\sim 10^{-9}$	-

case of atom interferometry, these transitions allow for both Bragg interferometry and single-photon clock atom interferometry schemes to be performed. Furthermore, the bosonic isotopes of these atoms have 0 spin, making them insensitive to external magnetic fields in their ground state.

Strontium is a very well established atomic source for a broad range of fundamental and applied physics experiments. In particular, the strongly forbidden $^1S_0$-$^3P_0$ transition is used for the world's most precise frequency measurements[16], and for measuring frequency ratios with fractional uncertainties below the 10^{-20} level[2]. For atom interferometry, large-momentum-transfer (LMT) atom interferometry has been demonstrated on both the $^1S_0$-$^1P_1$ and $^1S_0$-$^3P_1$ transitions in Bragg configurations[5,17], as well as on a single-photon scheme with the $^1S_0$-$^3P_1$ transition[9]. Moreover, clock atom interferometry on the $^1S_0$-$^3P_0$ transition has been demonstrated as experimentally feasible in gradiometer and gravimeter configurations[7,8]. Strontium is also suitable for trapped atom interferometry schemes that make use of Bloch oscillations to extend the interferometry time T without increasing the spatial size of the interferometer[18,19], with the ^{88}Sr isotope an especially interesting candidate due to its small negative scattering length allowing for long-lived oscillations without decoherence induced by inter-atomic collisions[20].

In contrast to Sr, Cd is only recently gaining attention as a practical atomic source. Much of this is due to the ground-state transitions lying in the ultraviolet regime. The requested UV light resonant with these transitions is technically challenging to produce and hampered early attempts to produce MOTs by causing photoionisation[21]. In principle, however, UV transitions offer multiple advantages for precision measurements with ultra-narrow transitions, including a reduced sensitivity to blackbody radiation which has long made Cd a candidate for atomic clocks, where blackbody radiation results in a leading systematic uncertainty[16]. Furthermore, for atom interferometry, the higher frequency of the UV transition results in a relatively larger momentum transfer per pulse and therefore increases intrinsic device sensitivity. Cadmium offers additional benefits as a test species, including the presence of eight naturally occurring isotopes[22], of which six are stable and the remaining two have half-lives greater than the lifetime of the universe[23] (Fig. 1). As six of these isotopes are bosons, this makes Cd an excellent candidate for precision frequency isotope shift spectroscopy[24,25], with applications in the probing of physics beyond the standard model[26].

As a test pair for atom interferometry, Cd and Sr benefit from the near 2:1 ratio of the main transitions of interest. This has fundamental advantages in a dual-species atom interferometer (see Section II B), but also enables technology transfer through the sharing of optics, cavities and master lasers (see Section III), which can reduce both cost and complexity of the experimental setup.

B. Enabled physics: WEP & Quantum interference of clocks

A dual-species atom interferometer enables a broad class of fundamental physics tests, but we focus here in particular on those relevant for our case of two atoms possessing clock transitions.

The weak equivalence principle (WEP) is a foundational postulate of general relativity and therefore modern physics, which states that an object undergoes free fall at a rate which is independent of its mass and internal structure. This principle has very recently been confirmed to the 10^{-15} level by comparing the free fall of two classical masses in space[27]. A dual-species atom interferometer which is sensitive to gravitational acceleration is a complimentary setting for testing WEP with quantum bodies, with recent measurements in a ^{85}Rb-^{87}Rb interferometer finding no violations down to the 10^{-12} level[1] and plans to test at the 10^{-13} level with a Rb-Yb interferometer under construction[28]. A Cd-Sr interferometer provides favourable conditions to perform these tests, due to the near 2:1 ratio of the transition frequencies, which e.g. by selecting Bragg orders with a factor 2 difference allows for almost equal k_{eff} and therefore interferometry times T[29] (Table II), which is important in minimising systematic phase shifts and allowing for common-mode rejection of vibrations[30]. Such an interferometer would also provide good sensitivity to WEP violations arising due to the constituents of matter having different rates of free fall. As shown in Table III, a Cd-Sr interferometer exhibits good estimated sensitivities[28] to such violations arising from both a dilaton model[31] and the standard model extension (SME) model[32]. The violation parameters for a range of Cd-Sr isotope pairs is comparable with other proposed dual-species systems, especially for SME, and the different isotope pairs afforded by Cd and Sr can be used to probe different linear combinations of these violating parameters.

Moreover, the presence of optical clock transitions in both Cd and Sr allows for WEP to be tested in a genuinely quantum mechanical framework, such as by preparing the atoms in a superposition of clock states. Although this has been performed already in Rb[33], the greatly increased energy separation will enhance the effect of any violation. In addition, there are very recent proposals for using atom interferometry with clock transitions and clock-state superpositions to test another aspect of Einstein's equivalence principle, namely local position invariance, via probing the universality of gravitational redshift[34–36] or the universality of clock rates[37].

Another physics goal is to look for time dilation effects of

TABLE II. Estimation of $k_{\rm eff}$ ratio (by e.g. using suitable Bragg order n for each atom) for dual-species interferometer tests of WEP. Setting $T_A = rT_B$, where $r = \sqrt{k_B^{\rm eff}/k_A^{\rm eff}}$, obtains the maximum common-mode noise rejection, as described in Ref. 29.

A	B	λ_A (nm)	λ_B (nm)	$r = \sqrt{k_B^{\rm eff}/k_A^{\rm eff}}$
Sr (^{1}P$_1$)	Cd (^{1}P$_1$)	460.9	228.8	1.004
Sr (^{3}P$_1$)	Cd (^{3}P$_1$)	689.4	326.1	1.028
Sr (^{3}P$_0$)	Cd (^{3}P$_0$)	698.4	332.1	1.025
Rb (D$_2$)	K (D$_2$)	780.2	766.7	1.009
Rb (D$_1$)	K (D$_1$)	794.9	770.1	1.016
Rb (D$_2$)	Yb (^{1}P$_1$)	780.2	398.9	1.011
K (D$_2$)	Yb (^{1}P$_1$)	766.7	398.9	1.002

systems prepared in a quantum superposition of states, which has been the source of much very recent theoretical discussion[38–41]. These questions are of particular interest due to the fundamental difference in the way that general relativity and quantum mechanics describe time[42] and it has been suggested that they may provide an insight into intrinsic decoherence mechanisms and the quantum-to-classical transition[43–46]. An atom interferometer has the potential to generate macroscopic spatial superpositions of atoms in an internal superposition of clock states, meaning the two arms of the interferometer can experience different time dilations, for example due to differing gravitational potentials. This can lead to a dephasing between the two interferometer arms which results in a modulation of interferometry fringe contrast[43]. This change in fringe visibility follows a periodic structure, with a full period of visibility loss and revival observed when $\Delta z \Delta T = \frac{c^2}{g\nu}$, where Δz is the difference in height between the two clock arms, ΔT is time spent at this height difference, and ν is the clock frequency[43]. The motivation for using a dual-species interferometer is that one atom can serve as a reference for the other, as fully eliminating visibility loss from other experimental sources (e.g. from background gas collisions) is very difficult. For example, $\Delta z \Delta T_{\rm Cd} = 10$ m·s and $\Delta z \Delta T_{\rm Sr} = 21$ m·s, meaning that Sr can serve as a reference for the faster decay of Cd, especially if laser noise can be made common-mode (see Section III C). A full decay and revival of the fringe pattern of Cd can be observed if, for example, $\Delta z = 2$ m and $\Delta T = 5$ s, which may be achievable in a hybrid fountain-trapped-atom system.

Recently, it has been shown that it is not necessary to measure the decay in fringe contrast directly, as the same physics leads to a phase shift in the interferometer[34]. The proposal is to use a doubly differential scheme, such as a Ramsey-Bordé interferometer, with the clock superposition applied at a variable time within the interferometer, and then measuring the differential phase shift between the ground and excited states. As well as being potentially less ambiguous than a loss of visibility, measuring such a differential phase shift should be more sensitive as the visibility loss is quadratically suppressed at small values of dephasing[34]. The expected change in differential phase shift between two different initialisation times Δt is $\Delta\phi_{\Delta t} = 2\pi\nu g \Delta z \Delta t / c^2$. Taking $\Delta z = 1$ cm, $\Delta t = 500$ ms then $\Delta\phi_{\Delta t}$ is 3.1 mrad and 1.5 mrad for Cd and Sr, respectively. Such resolution should in principle be attainable for atom interferometers with $\sim 10^6$ atoms and current technology, e.g. in a 2-m fountain. Nevertheless, achieving the required variable clock initialisation will require some significant technical challenges due to the requirement to create a superposition of clock states without imparting momentum[34], although a slightly modified scheme may mitigate some of these technical problems[47].

TABLE III. Estimated sensitivity parameters to WEP violations of selected dual-species Cd-Sr, Sr-Sr, and Cd-Cd in free-fall tests. For brevity, only some isotope combinations are shown and the Rb-Rb, Rb-K, and Rb-Yb values, originally reported in Ref. 28, are given for comparison. The first set of quoted values arise from the difference in the effective charges calculated from the composition of a test particle where $\eta_{AB} \cong D_1 \Delta Q'^1_{AB} + D_2 \Delta Q'^1_{AB}$, with η_{AB} the Eötvös ratio and D_1 and D_2 parameters to be constrained, following the model in Ref. 31. The second set arise from a difference in the defined violation parameters for matter $\Delta f_{\pm n}$ and antimatter $\Delta \bar{f}_{\pm n}$ linked to neutron excess and total baryon number, with $\eta_{AB} \cong \Delta f_{-n} + \Delta f_{+n} + \Delta \bar{f}_{-n} + \Delta \bar{f}_{+n}$, following the model in Ref. 32. For both cases, larger absolute values of these parameters lead to larger WEP violations.

A	B	$\Delta Q'^1_{AB}$ $\times 10^4$	$\Delta Q'^2_{AB}$ $\times 10^4$	Δf_{-n} $\times 10^2$	Δf_{+n} $\times 10^4$	$\Delta \bar{f}_{-n}$ $\times 10^5$	$\Delta \bar{f}_{+n}$ $\times 10^4$
^{87}Sr	^{106}Cd	-6.54	-3.99	1.66	-2.99	42.20	-1.98
^{87}Sr	^{113}Cd	-3.71	-6.11	-1.19	-1.13	25.03	-0.25
^{87}Sr	^{114}Cd	-2.62	-6.95	-2.30	-2.11	20.71	-1.22
^{88}Sr	^{108}Cd	-6.12	-4.23	1.31	-2.95	36.28	-1.87
^{88}Sr	^{113}Cd	-4.14	-5.72	-0.69	-3.17	14.22	-2.10
^{88}Sr	^{114}Cd	-3.77	-6.01	-1.07	-3.74	15.50	-2.72
^{84}Sr	^{88}Sr	1.77	-1.59	-2.09	2.71	-11.21	2.27
^{87}Sr	^{88}Sr	0.42	-0.39	-0.49	2.04	10.81	11.85
^{106}Cd	^{116}Cd	3.92	-2.96	-3.96	0.88	-21.49	0.76
^{108}Cd	^{116}Cd	3.07	-2.34	-3.12	-1.19	-26.38	-1.20
^{85}Rb	^{87}Rb	0.84	-0.79	-1.01	1.81	1.04	1.67
^{39}K	^{87}Rb	-6.69	-23.69	-6.31	1.90	-62.30	0.64
^{87}Rb	^{170}Yb	-12.87	-13.92	-1.36	-8.64	86.00	-5.46

III. LASER SYSTEM ARCHITECTURE

The laser systems for cooling and trapping and performing atom interferometry on cadmium and strontium are shown in Fig. 2 and summarised below, grouped by transition. Due to the prevalence of UV light, the systems have been constructed in a clean laboratory environment.

A. Laser systems for the ^{1}S$_0$-^{1}P$_1$ transition

The laser system for addressing the ^{1}S$_0$-^{1}P$_1$ transitions has been described before in detail[24], though we provide a brief

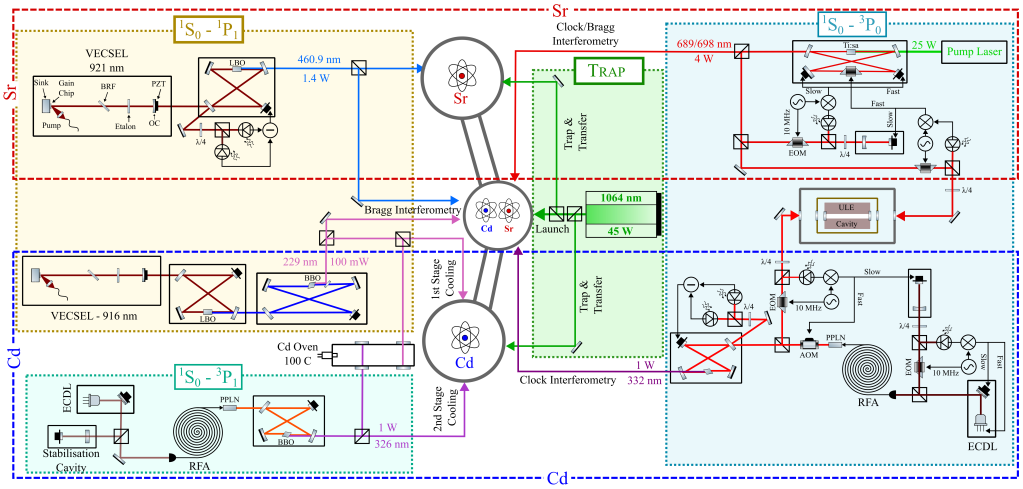

FIG. 2. Conceptual overview and basic design of the developed laser systems for Cd (dashed blue box) and Sr (dashed red box). Full details are given in the text and references, but the laser systems are grouped by transition to highlight the common design features. For the $^1S_0$-$^1P_1$ transition, both lasers are based on a common master VECSEL design, which is frequency doubled in a stabilised resonant bow-tie cavity (see Sr portion for details). The produced 461 nm is used directly for Sr, while the Cd system is doubled again to 229 nm. For $^1S_0$-$^3P_0$ clock transition, both the lasers can be locked to the same ULE cavity. The 698 nm light for Sr is derived from a Ti:sapph laser, which is pre-stabilised to a medium finesse cavity. To produce the 332 nm for Cd, an ECDL serves as a master which is amplified and frequency quadrupled. The ECDL is pre-stabilised to a medium finesse cavity, with further stabilisation to the ULE cavity performed on the doubled light at 664 nm. The $^1S_0$-$^3P_1$ transition laser for Cd follows the same design as the Cd clock laser, but without the additional stabilisation to the ULE cavity. To perform interferometry on the $^1S_0$-$^3P_1$ transition of Sr, the Ti:sapph laser can be tuned to 689 nm. A 45-W commercial 1064-nm laser will be used to perform an optical dipole trap, atom transfer and atom launching (green box).

summary here. Due to the near 2:1 ratio of these transitions for Cd and Sr, a common master laser design is employed, namely a wavelength-tunable vertical-external-cavity surface-emitting laser (VECSEL) frequency-doubled in a lithium triborate (LBO, LiB_3O_5) crystal placed at the tight focus of a resonant bow-tie cavity. Due to the excellent spatial mode quality and narrow linewidth of the VECSEL, efficient coupling to the cavity is readily achieved, a major improvement on systems based on tapered amplifiers. This design produces the required 461 nm light for addressing the $^1S_0$-$^1P_1$ transition of Sr directly, with a maximum of 1.4 W produced.

For Cd a further doubling stage to the deep-UV 229 nm is required. This regime remains highly challenging, especially for continuous-wave systems, despite recent progress at nearby wavelengths in terms of power and optical coatings[48,49]. For this reason, a large doubling cavity is employed, trading efficiency for stability, by increasing the size of the waist inside the doubling beta-barium borate crystal (BBO, β-BaB_2O_4), which is Brewster cut to remove the need for optical coatings which could be damaged by the UV. A maximum of 100 mW output has been achieved from this system. Further increasing the power and stability of the 229 nm light remains a long-term goal, although this power level is already sufficient for cooling and trapping[50].

B. Laser systems for the $^1S_0$-$^3P_1$ transition

The developed laser system for the $^1S_0$-$^3P_1$ transition of Cd will be used for laser cooling and trapping and for Bragg interferometry. It has been described before in detail[51]. In brief, however, a homebuilt external-cavity diode laser (ECDL) based on a gain chip emitting $\sim$ 80 mW at 1304.8 nm is amplified in a Raman fibre amplifier (RFA) up to powers exceeding 10 W, before being doubled in a periodically-poled lithium niobate crystal (PPLN, MgO:$LiNbO_3$), giving output powers of $\sim$3 W in the red. This red light is coupled to a resonant bow-tie cavity, stabilised with the Hänsch-Couillaud method, with a Brewster-cut BBO crystal placed at the tight focus. Total produced UV powers can reach up to 1 W following this doubling stage. In order to assure a narrow linewidth, the master laser is stabilised to a Fabry-Pérot cavity cavity (10 cm long, $\mathscr{F} \sim 10^4$) using the Pound-Drever-Hall (PDH) method, with measured in-loop linewidths on the kHz level. Fast feedback (>100 kHz) is achieved by feeding back directly to the diode current, while slow feedback is directed to the piezoelectric transducer (PZT) controlling the cavity length. The suitability of this system for addressing the 67-kHz-wide $^1S_0$-$^3P_1$ transition of Cd has been demonstrated by performing isotope-shift spectroscopy on a Cd beam and, especially, saturation-absorption spectroscopy.

For performing interferometry with the $^1S_0$-$^3P_1$ transition of Sr, a commercial Ti:sapph laser system, discussed in more detail below in Section III C, has been acquired. This system can give up to 4 W at 689 nm, representing a major improvement compared to the tapered-amplifier systems previously used for Bragg interferometry on this transition[5]. Such laser-diode-based systems will still be employed for the laser cooling and trapping to be performed on this transition, due to the considerably reduced optical power requirements.

C. Laser systems for the $^1S_0$-$^3P_0$ clock transition

The laser systems for the $^1S_0$-$^3P_0$ transitions of Cd and Sr have been described before in detail[52]. As with the case of the $^1S_0$-$^1P_1$ transition lasers, here we again make use of the near 2:1 ratio of the wavelengths by using the same super-high-finesse ultra-low-expansion (ULE) Fabry-Pérot cavity to stabilise both laser down towards the Hz level. The performance of this cavity has previously been demonstrated for Sr[53], but it is also suitable for stabilising the harmonic 664 nm light of the Cd transition. In this case, we measure $\mathscr{F}_{664} = 1.3 \times 10^5$, compared to $\mathscr{F}_{698} = 4.1 \times 10^5$ when operating at 698 nm. One advantage of this system, is that if both wavelengths can be coupled simultaneously in a counter-propagating scheme, then they will share common cavity-mode noise, which may be cancellable in a differential scheme[54].

The clock laser for Cd is very similar to the system described above except that an acousto-optical modulator (AOM) is used on the 664 nm with the first-order diffracted beam sent to the doubling cavity. A fraction of this first order beam is also coupled to the ULE cavity and an error signal derived using the PDH technique. This error signal is used to steer the pre-stabilisation Fabry-Pérot cavity via a mirror mounted on a PZT, holding the laser stable at low frequencies. Additional high frequency feedback is provided to the AOM, up to around a 50 kHz bandwidth. The measured in-loop error signal implies a linewidth of 2 Hz for the 664 nm light sent to the doubling cavity. As above, total produced UV powers are $\sim$1 W and Rabi frequencies $\Omega/2\pi \geq$kHz should be achievable with an interferometry beam with 5 mm radius.

Instead for Sr, a commercial Ti:sapph laser system is used, which is pumped by a 25 W CW laser at 532 nm. An intracavity electro-optical modulator (EOM) is inserted to increase the feedback bandwidth ($\sim$300 kHz) and in this configuration 4 W of output optical power at 698 nm is produced. Similarly to the case for the Cd setup, the Ti:sapph is first stabilised to a medium finesse Fabry-Pérot cavity via PDH locking, with feedback sent to two PZT actuated mirrors in the Ti:sapph cavity. The error signal from the ULE cavity is then sent to the PZT controlling the medium-finesse cavity length at low frequencies and to the EOM at high frequencies. The measured in-loop linewidth of 10 Hz means the laser should be capable of driving fast and efficient Rabi cycles ($\Omega/2\pi \sim 2$ kHz) even with a large beam radius (5 mm).

IV. EXPERIMENTAL DESIGN & CONSIDERATIONS

A. Cold atom apparatus & fountain

The two species will be independently prepared before being transferred together into the same chamber where they will be launched in a fountain configuration up a DN100CF tube. The preparation of cold Sr is well established, whereas only a few demonstrations of cold cadmium exist[21,25,50]. For this reason, a state-of-the-art cold cadmium apparatus has been designed and thoroughly numerically simulated, inspired by systems for producing continuous cold Sr[55]. The design and simulation have very recently been reported in full detail[56], but briefly, Cd will be loaded from an atomic beam into a 2D MOT using the 229 nm transition, before being slowly pushed down to a 3D MOT on the 326 nm transition placed $\sim$35 cm below. This design allows for atoms to be continuously loaded into the intercombination-transition MOT, whose Doppler temperature is 1.6 μK, away from the aggressive and high energy 229 nm photons. The estimated loading rate into the 3D MOT is $\sim 3 \times 10^7$ atoms/s. Although atom interferometry in 1-m fountains is possible with μK temperatures[33], further cooling following the MOT stage will be performed in independent optical dipole traps at 1064 nm, following which the atoms will be transferred to the main science chamber and brought together for interferometry. Quantum-degenerate samples have been produced for all isotopes of Sr[57], but neither this technique nor measurements of cold-collisional cross sections have been performed for Cd. The presence of eight isotopes of Cd means, however, that it should be possible to find an isotope with suitable quantum miscibility.

B. Atom launching

An important requirement for an accurate dual-species atom interferometer is that the two species are prepared with the same launch velocity. Although this can be most easily achieved by dropping the atoms, interferometry time is maximised by launching in a fountain. Approximately equal launch velocities can be achieved by using a lattice launch, for example with a far-off-resonant dipole trap[7]. We propose to use a 45 W 1064 nm laser to generate the lattice, as this can make a deep trap for both Cd and Sr simultaneously[56]. The launch process can be understood as a series of Bloch oscillations which impart momentum $2\hbar k_L$, where k_L is the lattice wavenumber[58]. For a lattice accelerated at a_L, the period of the Bloch oscillations is given by $\tau_B = 2\hbar k_L / m a_L$, where m is the mass of the atom. There will therefore be a small difference in the launch velocity for different Cd and Sr isotopes arising from their mass difference and a loss in atom number due to unmatched oscillation frequencies resulting in some isotopes being launched in a momentum-state superposition. However, these effects can be minimised by appropriately selecting the launch characteristics. For example, for an interferometer utilising the two most abundant isotopes, ^{114}Cd and ^{88}Sr and with the lattice accelerated over a 10 cm region, a launch acceleration chosen to match exactly $N_{\mathrm{Cd}} = 631$ os-

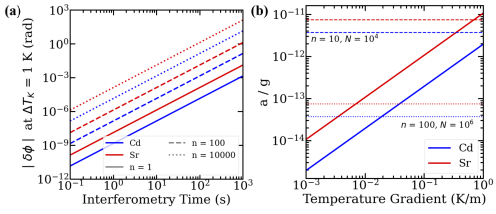

FIG. 3. The effect of blackbody radiation induced phase shifts. In all cases the ambient temperature is assumed to be 300 K, the interferometry time $T = 500$ ms and red denotes Sr and blue Cd. (a) The magnitude of the phase shift arising due to a change in temperature of 1 K in a clock atom interferometer. Different lines represent different LMT cases: solid lines, $n = 1$; dashed lines, $n = 100$; and dotted lines, $n = 10^4$. (b) The acceleration in units g of the phase shift in a Bragg interferometer operating on the $^1S_0$-$^1P_1$ transition (solid lines) in a temperature gradient of 0.1 K/m. Dashed lines show the atom shot noise limit for $n = 10$ and $N = 10^4$ atoms, and dotted lines the case for $n = 100$ and $N = 10^6$ atoms.

cillations results in $N_{Sr} \approx 487$ and to an apogee of $\sim$1 m. In this case, most of the the ^{88}Sr atoms will be launched in the desired momentum state and the two isotopes will have a different launch velocities of just $\Delta v_L = 0.2$ mm/s. The velocities of these clouds can then be more closely matched by using the velocity-selective nature of the interferometry beams. A WEP test at the 10^{-12} level used this method to achieve $\Delta v < 60\ \mu$m/s following a launch with $\Delta v_L < 1$ mm/s[1], which compares well with our estimate. The systematic effect arising from any remaining initial kinematic differences can be reduced by using an appropriate interferometry pulse sequence[59].

C. Role of blackbody radiation

As discussed in Section II A, a key motivation for using Cd for precision measurements is its reduced sensitivity to blackbody radiation (BBR). Although this has traditionally been considered in the context of atomic frequency standards, BBR can also lead to non-negligible shifts in atom interferometry[60] and has led to careful temperature monitoring being installed on some very-long baseline systems[61].

The frequency shift of a transition can be characterised according to $\delta\nu/\nu_0 = \beta\,(T_K/300\ \mathrm{K})^4$ where ν_0 is the unperturbed frequency and T_K the ambient temperature. The coefficient β is atom specific, with respective values of -2.8×10^{-16} and -5.5×10^{-15} for the $^1S_0$-$^3P_0$ optical clock transition of Cd[62] and Sr[63]. This results in static frequency shifts of -0.25 Hz and -2.4 Hz at $T_K = 300$ K, respectively, making Cd an order of magnitude less sensitive. For clock atom interferometers, the phase shift depends directly on the transition frequency as $\Delta\phi \sim 2\pi\nu g T^2/c$, so the BBR shift will translate directly into a change of interferometer phase[64]. More interesting than a static phase shift, however, are changes in temperature, either spatial or temporal, which could mimic a genuine signal of physical interest. A full analysis would have to consider the frequency spectra of the signal and the temperature fluctuations, but an idea of the problem can be achieved by considering $\delta\phi/\delta T_K$, as shown in Fig. 3 for the case of temperature changes of $\delta T_K = 1$ K about $T_K = 300$ K. As can be seen, such phase shifts can become considerable (>mrad) at long interferometry times and with large-momentum transfer and for this reason it has been suggested to use a three-loop interferometry sequence[11]. As $\delta\phi/\delta T_K \propto \beta\nu_0$, the effect is an order of magnitude less for Cd compared to Sr.

Blackbody radiation will also affect atom interferometers based on Bragg beams, where the atom stays in the ground electronic $^1S_0$ state throughout the interferometry sequence. Here the mechanism is a force arising due to any gradients in the a.c. Stark shift induced by the BBR field. The relevant parameter is therefore the static polarizability of the ground state α_0, which is $\alpha_{Cd} = 46.53$ a.u. and $\alpha_{Sr} = 197.2$ a.u. for Cd[50] and Sr[63], respectively. For a cylindrical vacuum chamber, the acceleration due to a variation of temperature along the symmetry axis z is given by $a(z) = \frac{1}{m}\frac{\partial}{\partial z}\frac{2\alpha_0\sigma T_K(z)}{c\varepsilon_0}$, where σ is the Stefan-Boltzmann constant[60]. As shown in Fig. 3, this can lead to potentially significant accelerations in comparison to the atom shot noise for realistic parameters, especially for the case of Sr, which is lighter and has a greater polarizability than Cd. For example, at $T_K = 300$ K and with $\partial T_K/\partial z = 0.1$ K/m, $a_{Cd} = 2$ pm/s^2 and $a_{Sr} = 10$ pm/s^2. Both these values are lower than in the case of Rb, where $a_{Rb} = 17$ pm/s^2. Such accelerations are close to the resolution achievable with state-of-the-art devices, which operate close to, but above, the shot-noise limit for 10^5 Rb atoms[1].

V. CONCLUSION & OUTLOOK

A dual-species Cd-Sr interferometer is being developed for fundamental physics tests with particular interest in exploiting the narrow intercombination transition afforded by these species. Work so far has primarily focused on the development and upgrading of the required laser and vacuum systems, including a set of three high-power, narrow-linewidth UV lasers for Cd. In the near future, cooling and trapping of Cd will be implemented and preliminary atom interferometry, which has yet to be demonstrated for this atom, will be performed. This phase will also involve rigorous measurements of the properties of different cold Cd isotopes, which are not currently available in the literature. Following this, experiments will begin on the full dual-species fountain Cd-Sr interferometer.

Although we have focused on a standard laboratory-scale experiment, many of the advantageous features identified here may also be of use for future very long baseline experiments, making Cd an attractive option for further research, especially as UV laser technology continues to mature.

ACKNOWLEDGMENTS

This work has been supported by the European Research Council, Grant No.772126 (TICTOCGRAV).

CONFLICT OF INTEREST STATEMENT

The authors have no conflicts to disclose.

DATA AVAILABILITY STATEMENT

Data sharing is not applicable to this article as no new data were created or analyzed in this study.

[1]P. Asenbaum, C. Overstreet, M. Kim, J. Curti, and M. A. Kasevich, "Atom-Interferometric Test of the Equivalence Principle at the 10^{-12} Level," Phys. Rev. Lett. **125**, 191101 (2020).
[2]T. Bothwell, C. J. Kennedy, A. Aeppli, D. Kedar, J. M. Robinson, E. Oelker, A. Staron, and J. Ye, "Resolving the gravitational redshift across a millimetre-scale atomic sample," Nature **602**, 420–424 (2022).
[3]A. D. Cronin, J. Schmiedmayer, and D. E. Pritchard, "Optics and interferometry with atoms and molecules," Rev. Mod. Phys. **81**, 1051–1129 (2009).
[4]G. M. Tino and M. A. Kasevich, *Atom Interferometry, Proceedings of the International School of Physics "Enrico Fermi," Course CLXXXVIII, Varenna 2013* (Società Italiana di Fisica and IOS Press, 2014).
[5]R. P. del Aguila, T. Mazzoni, L. Hu, L. Salvi, G. M. Tino, and N. Poli, "Bragg gravity-gradiometer using the $^1S_0 \rightarrow {}^3P_1$ intercombination transition of ^{88}Sr," New J. Phys. **20**, 043002 (2018).
[6]B. Plotkin-Swing, D. Gochnauer, K. E. McAlpine, E. S. Cooper, A. O. Jamison, and S. Gupta, "Three-Path Atom Interferometry with Large Momentum Separation," Phys. Rev. Lett. **121**, 133201 (2018).
[7]L. Hu, N. Poli, L. Salvi, and G. M. Tino, "Atom Interferometry with the Sr Optical Clock Transition," Phys. Rev. Lett. **119**, 263601 (2017).
[8]L. Hu, E. Wang, L. Salvi, J. N. Tinsley, G. M. Tino, and N. Poli, "Sr atom interferometry with the optical clock transition as a gravimeter and a gravity gradiometer," Classical and Quantum Gravity **37**, 014001 (2020).
[9]J. Rudolph, T. Wilkason, M. Nantel, H. Swan, C. M. Holland, Y. Jiang, B. E. Garber, S. P. Carman, and J. M. Hogan, "Large Momentum Transfer Clock Atom Interferometry on the 689 nm Intercombination Line of Strontium," Phys. Rev. Lett. **124**, 083604 (2020).
[10]L. Badurina *et al.*, "AION: an atom interferometer observatory and network," Journal of Cosmology and Astroparticle Physics **2020**, 011–011 (2020).
[11]M. Abe *et al.*, "Matter-wave Atomic Gradiometer Interferometric Sensor (MAGIS-100)," Quantum Science and Technology **6**, 044003 (2021).
[12]M.-S. Zhan *et al.*, "ZAIGA: Zhaoshan long-baseline atom interferometer gravitation antenna," International Journal of Modern Physics D **29**, 1940005 (2020).
[13]G. M. Tino *et al.*, "SAGE: A proposal for a space atomic gravity explorer," The European Physical Journal D **73** (2019), 10.1140/epjd/e2019-100324-6.
[14]Y. A. El-Neaj *et al.*, "AEDGE: Atomic Experiment for Dark Matter and Gravity Exploration in Space," EPJ Quantum Technology **7** (2020), 10.1140/epjqt/s40507-020-0080-0.
[15]A. Wicht, E. Sarajlic, J. M. Hensley, and S. Chu, "Phase shifts in precision atom interferometry due to the localization of atoms and optical fields," Phys. Rev. A **72**, 023602 (2005).
[16]T. Bothwell, D. Kedar, E. Oelker, J. M. Robinson, S. L. Bromley, W. L. Tew, J. Ye, and C. J. Kennedy, "JILA SrI optical lattice clock with uncertainty of 2.0×10^{-18}," Metrologia **56**, 065004 (2019).
[17]T. Mazzoni, X. Zhang, R. Del Aguila, L. Salvi, N. Poli, and G. M. Tino, "Large-momentum-transfer Bragg interferometer with strontium atoms," Phys. Rev. A **92**, 053619 (2015).
[18]X. Zhang, R. P. del Aguila, T. Mazzoni, N. Poli, and G. M. Tino, "Trapped-atom interferometer with ultracold Sr atoms," Phys. Rev. A **94**, 043608 (2016).
[19]V. Xu, M. Jaffe, C. D. Panda, S. L. Kristensen, L. W. Clark, and H. Müller, "Probing gravity by holding atoms for 20 seconds," Science **366**, 745–749 (2019).
[20]N. Poli, F.-Y. Wang, M. G. Tarallo, A. Alberti, M. Prevedelli, and G. M. Tino, "Precision Measurement of Gravity with Cold Atoms in an Optical Lattice and Comparison with a Classical Gravimeter," Phys. Rev. Lett. **106**, 038501 (2011).
[21]K.-A. Brickman, M.-S. Chang, M. Acton, A. Chew, D. Matsukevich, P. C. Haljan, V. S. Bagnato, and C. Monroe, "Magneto-optical trapping of cadmium," Phys. Rev. A **76**, 043411 (2007).
[22]M. Berglund and M. E. Wieser, "Isotopic compositions of the elements 2009 (IUPAC Technical Report)," Pure and Applied Chemistry **83**, 397–410 (2011).
[23]F. Kondev, M. Wang, W. Huang, S. Naimi, and G. Audi, "The NUBASE2020 evaluation of nuclear physics properties," Chinese Physics C **45**, 030001 (2021).
[24]J. N. Tinsley, S. Bandarupally, J.-P. Penttinen, S. Manzoor, S. Ranta, L. Salvi, M. Guina, and N. Poli, "Watt-level blue light for precision spectroscopy, laser cooling and trapping of strontium and cadmium atoms," Opt. Express **29**, 25462–25476 (2021).
[25]B. Ohayon, S. Hofsäss, J. E. Padilla-Castillo, S. C. Wright, G. Meijer, S. Truppe, K. Gibble, and B. K. Sahoo, "Isotope shifts in cadmium as a sensitive probe for physics beyond the standard model," New Journal of Physics **24**, 123040 (2022).
[26]I. Counts, J. Hur, D. P. L. Aude Craik, H. Jeon, C. Leung, J. C. Berengut, A. Geddes, A. Kawasaki, W. Jhe, and V. Vuletić, "Evidence for Nonlinear Isotope Shift in Yb^+ Search for New Boson," Phys. Rev. Lett. **125**, 123002 (2020).
[27]P. Touboul *et al.* (MICROSCOPE Collaboration), "*MICROSCOPE* Mission: Final Results of the Test of the Equivalence Principle," Phys. Rev. Lett. **129**, 121102 (2022).
[28]J. Hartwig, S. Abend, C. Schubert, D. Schlippert, H. Ahlers, K. Posso-Trujillo, N. Gaaloul, W. Ertmer, and E. M. Rasel, "Testing the universality of free fall with rubidium and ytterbium in a very large baseline atom interferometer," New Journal of Physics **17**, 035011 (2015).
[29]G. Varoquaux, R. A. Nyman, R. Geiger, P. Cheinet, A. Landragin, and P. Bouyer, "How to estimate the differential acceleration in a two-species atom interferometer to test the equivalence principle," New Journal of Physics **11**, 113010 (2009).
[30]B. Barrett, L. Antoni-Micollier, L. Chichet, B. Battelier, P.-A. Gominet, A. Bertoldi, P. Bouyer, and A. Landragin, "Correlative methods for dual-species quantum tests of the weak equivalence principle," New Journal of Physics **17**, 085010 (2015).
[31]T. Damour, "Theoretical aspects of the equivalence principle," Classical and Quantum Gravity **29**, 184001 (2012).
[32]M. A. Hohensee, H. Müller, and R. B. Wiringa, "Equivalence Principle and Bound Kinetic Energy," Phys. Rev. Lett. **111**, 151102 (2013).
[33]G. Rosi, G. D'Amico, L. Cacciapuoti, F. Sorrentino, M. Prevedelli, M. Zych, Č. Brukner, and G. M. Tino, "Quantum test of the equivalence principle for atoms in coherent superposition of internal energy states," Nature Communications **8**, 15529 (2017).
[34]A. Roura, "Gravitational Redshift in Quantum-Clock Interferometry," Phys. Rev. X **10**, 021014 (2020).
[35]C. Ufrecht, F. Di Pumpo, A. Friedrich, A. Roura, C. Schubert, D. Schlippert, E. M. Rasel, W. P. Schleich, and E. Giese, "Atom-interferometric test of the universality of gravitational redshift and free fall," Phys. Rev. Res. **2**, 043240 (2020).
[36]F. Di Pumpo, C. Ufrecht, A. Friedrich, E. Giese, W. P. Schleich, and W. G. Unruh, "Gravitational Redshift Tests with Atomic Clocks and Atom Interferometers," PRX Quantum **2**, 040333 (2021).
[37]F. Di Pumpo, A. Friedrich, C. Ufrecht, and E. Giese, "Universality-of-clock-rates test using atom interferometry with T^3 scaling," Phys. Rev. D **107**, 064007 (2023).
[38]A. J. Paige, A. D. K. Plato, and M. S. Kim, "Classical and nonclassical time dilation for quantum clocks," Phys. Rev. Lett. **124**, 160602 (2020).
[39]S. Khandelwal, M. P. Lock, and M. P. Woods, "Universal quantum modifications to general relativistic time dilation in delocalised clocks,"

Quantum **4**, 309 (2020).
[40]A. R. H. Smith and M. Ahmadi, "Quantum clocks observe classical and quantum time dilation," Nature Communications **11**, 5360 (2020).
[41]P. T. Grochowski, A. R. H. Smith, A. Dragan, and K. Dębski, "Quantum time dilation in atomic spectra," Phys. Rev. Research **3**, 023053 (2021).
[42]P. A. Bushev, J. H. Cole, D. Sholokhov, N. Kukharchyk, and M. Zych, "Single electron relativistic clock interferometer," New Journal of Physics **18**, 093050 (2016).
[43]M. Zych, F. Costa, I. Pikovski, and Č. Brukner, "Quantum interferometric visibility as a witness of general relativistic proper time," Nature Communications **2**, 505 (2011).
[44]I. Pikovski, M. Zych, F. Costa, and Č. Brukner, "Universal decoherence due to gravitational time dilation," Nature Physics **11**, 668–672 (2015).
[45]M. Carlesso and A. Bassi, "Decoherence due to gravitational time dilation: Analysis of competing decoherence effects," Physics Letters A **380**, 2354–2358 (2016).
[46]K. E. Khosla and N. Altamirano, "Detecting gravitational decoherence with clocks: Limits on temporal resolution from a classical-channel model of gravity," Phys. Rev. A **95**, 052116 (2017).
[47]A. Roura, C. Schubert, D. Schlippert, and E. M. Rasel, "Measuring gravitational time dilation with delocalized quantum superpositions," Phys. Rev. D **104**, 084001 (2021).
[48]Z. Burkley, L. de Sousa Borges, B. Ohayon, A. Golovizin, J. Zhang, and P. Crivelli, "Stable high power deep-uv enhancement cavity in ultra-high vacuum with fluoride coatings," Opt. Express **29**, 27450–27459 (2021).
[49]J. C. Shaw, S. Hannig, and D. J. McCarron, "Stable 2 W continuous-wave 261.5 nm laser for cooling and trapping aluminum monochloride," Opt. Express **29**, 37140–37149 (2021).
[50]A. Yamaguchi, M. S. Safronova, K. Gibble, and H. Katori, "Narrow-line Cooling and Determination of the Magic Wavelength of Cd," Phys. Rev. Lett. **123**, 113201 (2019).
[51]S. Manzoor, J. N. Tinsley, S. Bandarupally, M. Chiarotti, and N. Poli, "High-power, frequency-quadrupled UV laser source resonant with the $^1S_0$-$^3P_1$ narrow intercombination transition of cadmium at 326.2 nm," Opt. Lett. **47**, 2582–2585 (2022).
[52]M. Chiarotti, J. N. Tinsley, S. Bandarupally, S. Manzoor, M. Sacco, L. Salvi, and N. Poli, "Practical Limits for Large-Momentum-Transfer Clock Atom Interferometers," PRX Quantum **3**, 030348 (2022).
[53]M. G. Tarallo, N. Poli, M. Schioppo, D. Sutyrin, and G. M. Tino, "A high-stability semiconductor laser system for a ^{88}Sr-based optical lattice clock," Applied Physics B: Lasers & Optics **103**, 17–25 (2011).
[54]E. Wang, G. Verma, J. N. Tinsley, N. Poli, and L. Salvi, "Method for the differential measurement of phase shifts induced by atoms in an optical ring cavity," Phys. Rev. A **103**, 022609 (2021).
[55]C.-C. Chen, R. González Escudero, J. Minář, B. Pasquiou, S. Bennetts, and F. Schreck, "Continuous Bose–Einstein condensation," Nature **606**, 683–687 (2022).
[56]S. Bandarupally, J. N. Tinsley, M. Chiarotti, and N. Poli, "Design and simulation of a source of cold cadmium for atom interferometry," Journal of Physics B: Atomic, Molecular and Optical Physics **56**, 185301 (2023).
[57]S. Stellmer, R. Grimm, and F. Schreck, "Production of quantum-degenerate strontium gases," Phys. Rev. A **87**, 013611 (2013).
[58]T. Kovachy, J. M. Hogan, D. M. S. Johnson, and M. A. Kasevich, "Optical lattices as waveguides and beam splitters for atom interferometry: An analytical treatment and proposal of applications," Phys. Rev. A **82**, 013638 (2010).
[59]A. Roura, "Circumventing Heisenberg's Uncertainty Principle in Atom Interferometry Tests of the Equivalence Principle," Phys. Rev. Lett. **118**, 160401 (2017).
[60]P. Haslinger, M. Jaffe, V. Xu, O. Schwartz, M. Sonnleitner, M. Ritsch-Marte, H. Ritsch, and H. Müller, "Attractive force on atoms due to blackbody radiation," Nature Physics **14**, 257–260 (2018).
[61]Étienne Clément Wodey, *Methods for Very Long Baseline Atom Interferometry*, Ph.D. thesis, Gottfried Wilhelm Leibniz Universität Hannover (2021).
[62]V. A. Dzuba and A. Derevianko, "Blackbody radiation shift for the $^1s_0$-$^3p_0$ optical clock transition in zinc and cadmium atoms," Journal of Physics B: Atomic, Molecular and Optical Physics **52**, 215005 (2019).
[63]S. G. Porsev and A. Derevianko, "Multipolar theory of blackbody radiation shift of atomic energy levels and its implications for optical lattice clocks," Phys. Rev. A **74**, 020502 (2006).
[64]P. W. Graham, J. M. Hogan, M. A. Kasevich, and S. Rajendran, "New Method for Gravitational Wave Detection with Atomic Sensors," Phys. Rev. Lett. **110**, 171102 (2013).